Structural and Mechanistic Studies on ThiO, a Glycine Oxidase Essential for Thiamin Biosynthesis in *Bacillus subtilis*[†,‡]

Ethan C. Settembre, Pieter C. Dorrestein, Joo-Heon Park, Amy M. Augustine, Tadhg P. Begley,* and Steven E. Ealick*

Department of Chemistry and Chemical Biology, Cornell University, Ithaca, New York 14853

Received September 27, 2002; Revised Manuscript Received January 22, 2003

ABSTRACT: The *thiO* gene of *Bacillus subtilis* encodes an FAD-dependent glycine oxidase. This enzyme is a homotetramer with a monomer molecular mass of 42 kDa. In this paper, we demonstrate that ThiO is required for the biosynthesis of the thiazole moiety of thiamin pyrophosphate and describe the structure of the enzyme with *N*-acetylglycine bound at the active site. The closest structural relatives of ThiO are sarcosine oxidase and D-amino acid oxidase. The ThiO structure, as well as the observation that *N*-cyclopropylglycine is a good substrate, supports a hydride transfer mechanism for the enzyme. A mechanistic proposal for the role of ThiO in thiazole biosynthesis is also described.

Thiamin pyrophosphate **13** plays a key role in the stabilization of acyl carbanion intermediates and is an essential cofactor in all living systems. The biosynthesis of thiamin is complex and is not yet well-understood. The thiazole and the pyrimidine moieties are synthesized in separate branches of the pathway and are coupled to form thiamin phosphate, which is phosphorylated to generate the active form of the cofactor. In some bacteria (e.g., *Escherichia coli*), the thiazole moiety is synthesized from cysteine, deoxy-D-xylulose 5-phosphate, and tyrosine in a set of reactions requiring ThiF, ThiS, ThiG, ThiH, ThiI, and IscS. In other bacteria (e.g., *Bacillus subtilis*), the thiazole moiety is synthesized from cysteine, deoxy-D-xylulose 5-phosphate, and glycine, and sequence analysis suggests that the biosynthesis is catalyzed by ThiF, ThiS, ThiG, ThiO, ThiI, and NifS (Figure 1) (*1*−*3*).

The specific reactions catalyzed by several of the thiazole biosynthetic proteins have now been identified. IscS is a PLP-utilizing enzyme that reacts with cysteine to give an active site persulfide (*2*). This persulfide adds to the carboxy-terminal acyladenylate of ThiS, and the resulting acyl disulfide undergoes a disulfide exchange reaction with Cys184 of ThiF to form a covalent ThiF−ThiS complex linked by an acyl disulfide linkage. This intermediate is likely to be the sulfur donor for the thiazole biosynthesis in *E. coli* (*4*). In addition to its role in the formation of the acyl disulfide, ThiF also catalyzes the formation of the acyl adenylate of ThiS (*5*). The specific reactions catalyzed by ThiG and ThiH have not yet been identified.

In *B. subtilis*, ThiS thiocarboxylate **3** rather than the ThiF−ThiS acyl disulfide is likely to be the immediate sulfur donor (TPB unpublished) and ThiF, ThiS, and ThiG are likely to have functions identical or very similar to those of the *E. coli* enzymes. However, ThiO and ThiH share no sequence similarity. These differences in substrate utilization and enzymatic requirements suggest subtle differences between the biosynthetic strategies for thiazole formation in *E. coli* and *B. subtilis*. However, these differences remain to be elucidated because thiazole biosynthesis has not yet been reconstituted in a cell free system.

ThiO (YjbR) was previously isolated as a homotetramer of 42 kDa subunits and shown to be an FAD-dependent glycine oxidase (*6*). Amine oxidases have been extensively studied, and the structures of sarcosine oxidase (*7*), D-amino acid oxidase (*8*, *9*), L-aspartate oxidase (*10*), and polyamine oxidase (*11*) have been reported. The mechanism for the reaction is still controversial, and mechanisms involving an electron transfer, a hydride transfer, and a covalent amine flavin adduct are all still considered possible. Sequence homology searches indicated that ThiO is 18−27% identical with the sarcosine oxidases and D-amino acid oxidases (*3*, *12*). These proteins are characterized by a conserved amino acid sequence of the FAD binding glutathione reductase 2 (GR_2)[1] family (*13*).

In this paper, we demonstrate that the glycine oxidase encoded by the *thiO* gene is essential for thiazole formation in *B. subtilis*, we describe mechanistic and structural studies on this enzyme, and we propose a role for ThiO in the biosynthesis of the thiazole moiety of thiamin.

[†] This work was supported by National Institutes of Health Grant DK44083 (to T.P.B.). S.E.E. is indebted to the W. M. Keck Foundation and the Lucille P. Markey Charitable Trust.

[‡] The Protein Data Bank entry for ThiO is 1NG4 and for the ThiO complex with *N*-acetylglycine is 1NG3.

* To whom correspondence should be addressed: Department of Chemistry and Chemical Biology, Cornell University, Ithaca, NY 14850. Telephone: (607) 255-7961. Fax: (607) 255-1227. E-mail: see3@cornell.edu or tbp2@cornell.edu.

[1] Abbreviations: SOX, sarcosine oxidase; DAAOX, D-amino acid oxidase; pkDAAOX, pig kidney D-amino acid oxidase; rgDAAOX, *Rhodotorula gracilis* D-amino acid oxidase; CIP, calf intestinal alkaline phosphatase; GR_2, glutathione reductase 2; PEG 2K MME, polyethylene glycol monomethyl ether 2000; CHESS, Cornell High Energy Synchrotron Source; LB, Luria−Bertani medium; DTT, dithiothreitol; APS, Advanced Photon Source; DXP, deoxy-D-xylulose 5-phosphate; FAD, flavin adenine dinucleotide; SeMet, selenomethionine.

10.1021/bi026916v CCC: $25.00
Published on Web 02/22/2003

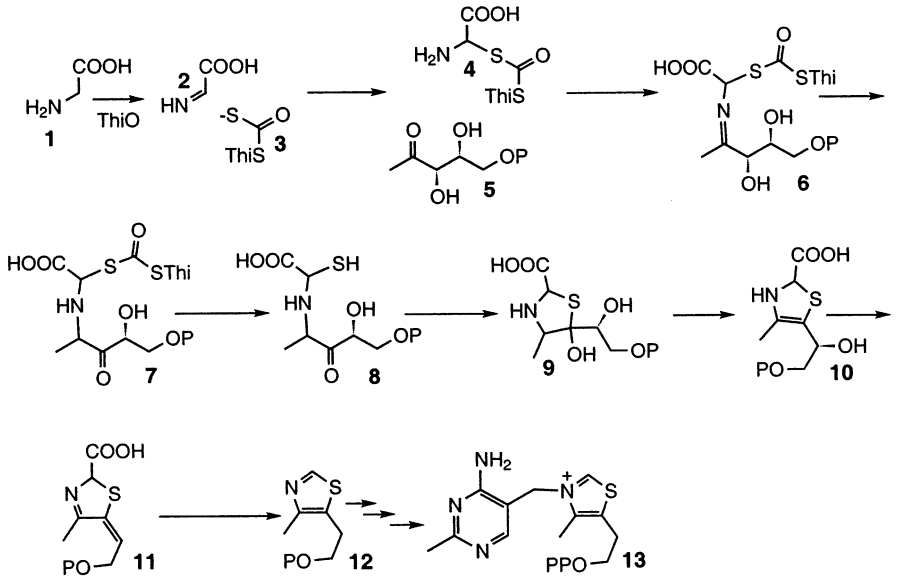

FIGURE 1: Mechanistic proposal for the role of ThiO in the biosynthesis of the thiazole moiety of thiamin pyrophosphate in *B. subtilis*.

MATERIALS AND METHODS

Chemical Reagents. Thiazole, glycine, cysteine, horseradish peroxidase, L-alanine [99% enantiomeric excess (ee)], D-alanine (99% ee), 1-amino-2-propanol, (*S*)-(+)-2-amino-1-propanol (97% ee), (*R*)-(+)-2-amiopropanol (97% ee), cyclopropylamine, and 2,2-dideuterioglycine (98% deuterated) were from Sigma-Aldrich. [2-^{13}C]Glycine was from Cambridge Isotope Laboratories, and phenol was from Mallinckrodt.

Growth Curves for ThiO$^-$ B. subtilis. The ThiO deficient *B. subtilis* was a gift from J. Errington (Oxford University, Oxford, England) (*14*). The fastest growing colonies on LB/erythromycin plates were used to inoculate 3 mL of minimal medium. After 24 h at 37 °C, the slowest growing culture was used to inoculate 50 mL of minimal medium. This culture was maintained at 37 °C for 24 h to starve the cells for thiamin and divided into two 25 mL cultures, and an additional 25 mL of minimal medium was added to each. Thiazole alcohol (2 μM) was added to one of the cultures. The absorbance at 595 nm was monitored to obtain the growth curves. Special precautions were taken to ensure that the flasks used for the growth curves had not been exposed to full medium, thiamin, or thiazole. One liter of minimal medium used for the growth curve contained 200 mL of 5× minimal salt solution, 20 mL of 20% glucose, 5 mL of 1% L-tryptophan, 50 mL of 4% L-glutamine, 2 mL of 2 mg/mL $FeCl_3$, 2 mL of 0.1 mg/mL $MnSO_4$, and 10 mL of the 100× trace elements. The 5× minimal salt solution contained 0.057 M K_2SO_4, 0.31 M $K_2HPO_4 \cdot 5H_2O$, 0.017 M sodium citrate, and 0.004 M $MgSO_4$ and was adjusted to pH 7 with 10 N NaOH. The 100× trace elements contained 0.55 g of $CaCl_2$, 0.17 g of $ZnCl_2$, 0.043 g of $CuCl_2 \cdot 2H_2O$, 0.06 g of $CoCl_2 \cdot 6H_2O$, and 0.06 g of $Na_2MoO_4 \cdot 2H_2O$ in 1 L of solution.

ThiO Overexpression. The *thiO* gene was PCR amplified from *B. subtilis* genomic DNA (strain CU1065) using the following primer pair: 5′-GCT AAA GGA GAT GCC ATA TGA AAA GGC ATT ATG AAG C-3′ (inserts an *Nde*I site at the start codon) and 5′-CGT CTT TAC CGT TCA GCT CGA GCA TCA TAT CTG AAC CGC C-3′ (inserts an *Xho*I site after the stop codon). The PCR product was completely digested with *Nde*I and *Xho*I, resulting in two fragments. One fragment, from an internal *Nde*I site to the engineered *Xho*I site, was ligated into similarly digested pET-16b to give pCLK810. This plasmid was digested with *Nde*I and dephosphorylated with CIP. The other fragment from the PCR product digest, from the engineered *Nde*I site to the internal *Nde*I site, was ligated into the cut and dephosphorylated pCLK810. Clones were screened for the direction of the insertion, and one with the correct orientation was named pCLK811 (*thiO* in pET-16b).

Protein Purification. The native protein was obtained by inoculating 1 L of LB and 100 μg/mL ampicillin with 5 mL of a saturated starter culture. The cells were grown at 37 °C until they reached an OD_{600} of ~0.6, at which point the temperature was lowered to 30 °C and the cells were induced with 500 μM isopropyl β-D-thiogalactoside. After induction for 4 h, the cells were spun down at 5000 rpm for 10 min and stored at −80 °C.

For production of the protein with selenomethione (SeMet) incorporated, the methionine auxotrophic strain of *E. coli*, B834(DE3) (Novagen), was transformed with pCLK811 and the cells were grown using growing conditions slightly varied from those described above. The 1 L of growth medium contained M9 salts supplemented with all amino acids (40 μg/mL each) except L-methionine, which was replaced with L-SeMet, 0.4% (w/v) glucose, 2 mM $MgSO_4$, 25 μg/mL $FeSO_4 \cdot 7H_2O$, 1 mM $CaCl_2$, 100 μg/mL ampicillin, 1 mM DTT, and a 1% BME vitamin solution (GibcoBRL). Also, the cells from the initial 5 mL starter culture were washed with the above medium, and used to start a 50 mL culture. This second culture was grown to an OD_{600} of ~0.6 and used to inoculate the larger 1 L culture. The rest of the expression was performed as described above.

All purification steps were carried out at 4 °C. All buffers contained 1 mM DTT for the protein with SeMet incorporated. The cells were resuspended in 20 mL of wash buffer [50 mM NaH_2PO_4, 300 mM NaCl, and 20 mM imidazole (pH 8.0)] and broken using a French press. The crude extract was centrifuged, and the resulting supernatant was mixed for 1 h with 500 μL of Ni-NTA beads (Novagen) equilibrated

with the wash buffer. The beads were then added to a polypropylene column and were washed with 300 mL of wash buffer. The column was first eluted with 20 mL of wash buffer containing 50 mM imidazole to remove weakly binding proteins. ThiO was eluted from the column using wash buffer containing 150 mM imidazole. After gel filtration using an Econo-Pac 10DG column (Bio-Rad) with elution with 50 mM Tris (pH 7.0), the protein was concentrated to 10 mg/mL using a 10 kDa cutoff concentrator (Amicon) and stored at −80 °C. Protein concentrations were determined by the Bradford method (*15*) using bovine serum albumin as the standard. The purity of ThiO was determined by Coomassie-stained SDS−PAGE and found to be greater than 99% (data not shown).

*Synthesis of Cyclopropylglycine (**15**).* Chloroacetic acid (50 mg, 0.53 mmol) was added at room temperature with stirring to cyclopropylamine (3 g, 53 mmol). After 3 days, the unreacted cyclopropylamine was removed by vacuum distillation. The resulting crude *N*-cyclopropylglycine was dissolved in methanol and then rotary evaporated to remove residual cyclopropylamine. The product was purified by recrystallization from a 33.9:33:33:0.1 chloroform/ethyl acetate/acetone/ethanol mixture, to give **15** as a white crystalline solid (37 mg, 61%): ^{1}H NMR (400 MHz, D_2O) δ 3.59 (2 H, s), 2.64 (1 H, m), 0.66 (4 H, m); ^{1}H NMR (400 MHz, 10 mM phosphate buffer in D_2O, pD 7.4) δ 3.49 (2 H, s), 2.54 (1 H, m), 0.15 (4 H, m); EI-MS (M^+) 116.1; EI-MS-MS (M^+) 116.1, 88.1, 70.2.

*Synthesis of Compounds **16**−**18**.* These were prepared in a manner similar to that of compound **15**. Compound **16**: ^{1}H NMR (D_2O, rotamer mixture) δ 3.55 (dd, 1 H), 3.35 (m, 3 H), 3.05 and 3.20 (sextet, 1 H), 1.01 and 1.04 (d, 3 H); EI-MS (M^+) 134.1; EI-MS-MS (M^+) 134.1, 116.1, 88.1, 70.2. Compound **17**: ^{1}H NMR (D_2O, rotamer mixture) δ 3.55 (dd, 1 H), 3.35 (m, 3 H), 3.05 and 3.20 (sextet, 1 H), 1.01 and 1.04 (d, 3 H); EI-MS (M^+) 134.0; EI-MS-MS (M^+) 134.0, 116.1, 88.1. Compound **18**: EI-MS (M^+) 134.0; EI-MS-MS (M^+) 134.0, 116.1, 88.1.

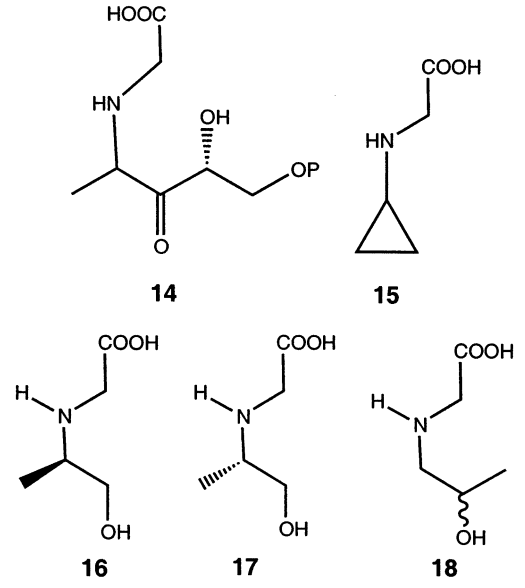

Enzyme Assays. ThiO activity was measured by monitoring hydrogen peroxide production as previously described (*6*). A typical reaction mixture contained 50 mM 4-aminoantipyrine, 5 units of horseradish peroxidase, 2 mM phenol, and 8 mM glycine or glycine analogue (compounds **15**−**18**) in 0.5 mL of 25 mM Tris-HCl (pH 7.8). The reaction was initiated by the addition of 25 μL of ThiO (8−12 mg/mL) and monitored over a period of 10 min using the increasing absorbance at 500 nm (ϵ = 5560 M^{-1} cm^{-1}). For kinetic characterization, various concentrations of glycine or its analogues were incubated with the enzyme and the initial rates were fitted to the Michaelis−Menten equation using Sigmaplot.

Characterization of the Glycine Oxidation Product. A solution of freshly prepared ThiO (0.35 mL, 3.4 mg/mL) and 2000 units of catalase were added to 4 mL of glycine or [2-^{13}C]glycine (10 mM) in 40 mM KP_i (pH 7.9). After 3 h, the reaction mixture was lyophilized, redissolved in D_2O (1 mL), centrifuged, and analyzed by NMR (400 MHz).

Characterization of the N-Cyclopropylglycine Oxidation Products. A stock solution (10 mM) of *N*-cyclopropylglycine in deuterated 10 mM phosphate buffer (pD 8.2) was prepared. ThiO [75 μL, 18 mg/mL in 20 mM phosphate buffer (pH 7.8)] was added to 0.75 mL of this stock solution, and the reaction was monitored using NMR with solvent suppression after 0, 3, 18, 36, and 72 h, at which time 75% of **15** was converted to formate, glyoxalate, and cyclopropylamine. Ring-opened products were not observed. Compound **15** was stable under these conditions in the absence of the enzyme.

Kinetics of Flavin Reduction. Glycine or deuterated glycine [150 μL, 400 mM in 200 mM Tris-HCl (pH 7.6) degassed by sonication under vacuum] was mixed 1:1 with ThiO (degassed by soniation under vacuum) (3.6 mg/mL**)** using a stopped flow instrument, and the absorbance decrease at 455 nm was recorded for 2−10 s at 0.002 s intervals. The stopped flow instrument was a Hi-Tech Scientific preparative Quench and stopped flow SHU PQ/SF-53 model with a Hi-Tech Scientific SU-40 spectrometer unit and Keithley Driverlinx software. The observation cell has a high-efficiency mixer with an optical path length of 2 mm and two emission windows (2 mm × 2 mm). The average dead time for this instrument is 16−20 ms. The kinetics were determined at room temperature. The data for each experiment were imported into Sigmaplot and fitted to a first-order exponential decay.

Stereochemistry of the ThiO-Catalyzed Oxidation. L-Alanine and D-alanine were tested as substrates using the hydrogen peroxide assay described above. Each reaction mixture contained 2 units/mL horseradish peroxidase, 100 mM 4-aminoantipyrine, 4 mM phenol, and 3−800 mM D-alanine or L-alanine in 500 μL. D-Alanine was a substrate, while L-alanine was not. To obtain an approximate relative rate for the two isomers, reaction mixtures containing 100 mM samples of L-alanine and D-alanine were incubated with ThiO and the hydrogen peroxide assay system for 4 h. No L-alanine oxidation was observed, giving k_D/k_L relative rates of ≥5000. Because the L-alanine sample was contaminated with 0.5% D-alanine, the rates were recorded after an initial incubation of 300 s to ensure removal of this contaminant.

Crystallization of ThiO. ThiO was crystallized using the hanging drop method with each drop containing 2 μL of protein and 1 μL of well solution. The protein concentration was 10 mg/mL, and the well solution for optimized conditions contained 18% polyethylene glycol monomethyl ether 2000 (PEG 2K MME) and 100 mM 4-(2-hydroxyethyl)-1-

piperazineethanesulfonic acid (pH 7.15). Crystals appeared within 1 week and grew to their maximum size (0.5 mm × 0.5 mm × 0.35 mm) in 2 weeks. Crystals were yellow, indicative of the presence of the oxidized FAD cofactor. Preliminary X-ray analysis showed that the crystals belong to space group $P6_122$ or $P6_522$ with the following unit cell dimensions: $a = 139.39$ Å and $c = 209.64$ Å. The crystals contain two monomers per asymmetric unit, corresponding to a solvent content of 60%.

The crystallization conditions for the native protein and protein with SeMet incorporated were essentially the same except that 1 mM DTT was added for the SeMet protein. In general, crystals of the SeMet protein were ~0.1 mm smaller in each direction. Crystals of the *N*-acetylglycine complex were prepared by adding 5 mM *N*-acetylglycine to the crystallization solution and 10 mM *N*-acetylglycine during cryoprotection. *N*-Acetylglycine is not a substrate and inhibits the enzyme.

For cryoprotection, the crystals were gently transferred to a stabilization solution that was similar to the mother liquor but with 30% PEG 2K MME. The crystals were then transferred into solutions with increasing ethylene glycol concentrations (1% steps until the final concentration of 11% was reached), frozen by plunging them into liquid nitrogen, and stored for later use. For the *N*-acetylglycine complex, 10 mM *N*-acetylglycine was present as well.

X-ray Data Collection and Processing. A two-wavelength data set was collected at the F2 station of the Cornell High Energy Synchrotron Source (CHESS) to 3.25 Å resolution. Following calibration of the beam using a Se foil, a fluorescence scan was taken on a SeMet-ThiO crystal. For data collection, one wavelength was chosen at the maximum of f' (edge) and the other was selected at the maximum of f'' (peak). The remote wavelength data were not collected because of crystal decay. Data were collected over 75° using 90 s for each 1° oscillation with a crystal to Quantum 4 CCD detector (Area Detector Systems Corp.) distance of 250 mm. Bijvoet pairs were measured after each 10° wedge using inverse beam geometry. Throughout data collection, wavelength calibration was checked and the camera was adjusted to maximize the flux as needed. The DENZO suite of programs was used for integration and scaling of the data (*16*). The inverse and direct beams were initially scaled together before the separate wavelengths were scaled together.

Single-wavelength data were taken at beamline 8-BM at the Advanced Photon Source (APS) using a Quantum 315 detector (Area Detector Systems Corp.) in binned format. Data were collected over a range of 120° using 20 s for each 0.5° oscillation at a crystal to detector distance of 340 mm. MOSFLM (*17*) was used for data integration, and SCALA (*18*) was used for scaling. All data collection statistics are summarized in Table 1.

Structure Determination. The initial Se atom positions were determined utilizing shake-and-bake direct methods (*19*) as implemented in SnB (*20*). The peak wavelength data were used to calculate normalized anomalous differences (ΔE) using the DREAR (*21*) suite of programs. A total of 2000 ΔE's with $\Delta E/\sigma$ (ΔE) values of >3.5 and 20 000 triplet invariants were used to carry out 1000 random trials with 80 cycles of phase refinement per trial. Five of these trials produced solutions as judged by the behavior of the shake-and-bake minimal function. From these phases, 18 of 24 expected Se atom positions were identified. These sites showed a noncrystallographic 2-fold axis perpendicular to a crystallographic 2-fold axis. The Se atom positions were input into CNS (*22*) and used for phasing. Data from both wavelengths were scaled together using CNS with the peak wavelength used as the reference. The initial phases were used to identify the six remaining Se atoms from a combination of anomalous difference Fourier and log-likelihood Fourier maps, and phases were recalculated using the 24 Se atom positions.

Table 1: Summary of Data Collection and Processing Statistics

	Se (CHESS F2)		(APS 8BM)	
	edge	peak	native	complex
wavelength (Å)	0.9793	0.9791	0.9791	0.9791
resolution (Å)	3.25	3.25	2.3	2.6
no. of reflections	281836	291076	647137	164553
no. of unique reflections	19316	19189	51731	34445
redundancy	14.6	15.2	12.4	4.6
completeness[a]	97.9 (96.7)	97.6 (97.1)	96.7 (96.7)	96.4 (96.4)
R_{sym} (%)[a,b]	10.3 (38.6)	10.3 (32.2)	9.4 (34.9)	6.8 (31.1)
I/σ[a]	7.6 (3.2)	8.0 (3.4)	20.7 (6.2)	17.9 (4.6)

[a] Values for the outer resolution shell are given in parentheses. Cornell High Energy Synchrotron Source (CHESS), MAD F2 data, 3.25 Å for edge and peak. Advanced Photon Source (APS) 8BM native ThiO data to 2.3 Å and *N*-acetylglycine complex data to 2.6 Å. [b] $R_{sym} = \sum\sum_i|I_i - \langle I\rangle|/\sum\langle I\rangle$, where $\langle I\rangle$ is the mean intensity of *N* reflections with intensities I_i and common indices *h*, *k*, and *l*.

Model Building and Structure Refinement. All model building was performed using the computer program O (*23*). Electron density maps were calculated for each possible space group, $P6_122$ or $P6_522$, and only the electron density for space group $P6_122$ showed features consistent with a protein structure. The map was further improved with the addition of the noncrystallographic symmetry (NCS) constraints and a protein mask that was created from a bones representation of the electron density using the program MAPMAN (*24*). The backbone was traced for residues 5−53, 60−181, and 197−360, and the second monomer was generated using NCS. At this stage, FAD molecules were clearly visible in the electron density of each monomer and were included in the model. Combining calculated phases with the initial phases improved the map in all regions so that the entire chain could be traced from residue 1 to 360 and side chains were included for each monomer. The refinement procedure involved successive rounds of rigid body refinement, simulated annealing refinement, temperature factor refinement, and model rebuilding.

In the native structure, some electron density for which we cannot account appeared above the isoalloxazine ring roughly in the position where the carboxyl group of *N*-acetylglycine was positioned in the complex. This density appeared to be too spread out to be a water molecule but not sufficiently spread out to be a series of water molecules. The density was modeled as a hydrogen peroxide molecule, one of the expected reaction products. The final refinement statistics are shown in Table 2.

RESULTS

ThiO⁻ Mutant. The ThiO⁻ mutant grown on minimal medium has an absolute requirement for the thiazole moiety of thiamin as illustrated in Figure 2.

Table 2: Refinement Statistics and Model Building

	ThiO	ThiO−*N*-acetylglycine
resolution (Å)	50−2.3	50−2.6
total no. of non-hydrogen atoms	6008	5924
no. of protein atoms	5688	5688
no. of water oxygen atoms	205	109
no. of ligand atoms	115	127
no. of reflections in refinement	53499	35656
no. of reflections in the test set	4375	1905
R factor[a] (%)	21.5	20.9
R_{free}[b] (%)	24.8	23.9
rms deviation from ideal geometry		
bonds (Å)	0.007	0.007
angles (deg)	1.3	1.4
Ramachandran plot		
most favored region (%)	86.4	84.0
additional allowed region (%)	12.5	15.0
generously allowed region (%)	0.8	0.5
disallowed region (%)	0.3	0.5
average *B* factor (Å^2)		
main chain	34.2	40.1
side chain	37.0	42.3
water	36.4	33.4
phosphate	61.7	64.0
ligand	38.7	66.1
FAD	21.5	25.4

[a] R factor $= \sum_{hkl}||F_{obs}| - k|F_{cal}||/\sum_{hkl}|F_{obs}|$, where F_{obs} and F_{cal} are the observed and calculated structure factors, respectively. [b] For R_{free}, the sum is extended over a subset of reflections excluded from all stages of refinement, 8% for native ThiO and 6% for the ThiO complex.

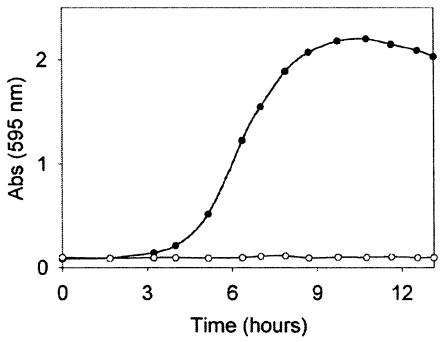

FIGURE 2: ThiO$^-$ complementation by thiazole alcohol after thiamin starvation of the cells for 48 h: (●) *B. subtilis* ThiO$^-$ in minimal medium with 2 μM thiazole alcohol added and (○) *B. subtilis* ThiO$^-$ in minimal medium without thiazole.

Product Characterization by NMR. When the enzyme-catalyzed oxidation of glycine or [2-^{13}C]glycine was analyzed by NMR, the gemdiol CH proton and the carbon of hydrated glyoxylate (the glycine imine hydrolysis product) were readily observed at 5.03 (^{1}H) and 89 ppm (^{13}C), respectively. When catalase was omitted from the reaction mixture, glyoxylate was oxidatively decarboxylated by hydrogen peroxide to formate, which exhibited signals at 172 ppm for the carbonyl carbon and at 8.2 ppm for the acyl proton. The glycine imine could be trapped by the addition of 4 mM cysteine (signal at 68 ppm when [2-^{13}C]glycine was used as the substrate). The 2,4-thiazolidine dicarboxylate was hydrolyzed to glyoxylate over a period of 2 days.

Substrate Analogues. Compounds **15**−**18** were synthesized and tested as substrates for glycine oxidase. The kinetic parameters for these compounds, as well as those for glycine, are given in Table 3. Cyclopropylglycine was a good substrate for glycine oxidase, and no time-dependent inactivation was observed. The apparent K_m and k_{cat} values are comparable to those of glycine. NMR analysis of the ThiO-catalyzed oxidation of the cyclopropylglycine reaction mixture demonstrated that the products were formate (8.2 ppm), hydrated glyoxalate (5.03 ppm), and cyclopropylamine (see Figure 3). Compounds **16** and **17** were poor substrates, while compound **18** was a good substrate. We are unable to give a structural explanation for the observation that analogues **15** and **18** are substrates while analogs **16** and **17** are not.

Table 3: Glycine Analogues as Alternative Substrates for ThiO

compound	k_{app} (min^{-1})	$K_{m(app)}$ (mM)
glycine	1.2 ± 0.09	1.12 ± 0.3
15	1.0 ± 0.07	1.17 ± 0.09
16	poor activity at 25 mM	not measured
17	poor activity at 25 mM	not measured
18	1.14 ± 0.06	3.0 ± 0.5
D-alanine	0.40 ± 0.01	162 ± 11
L-alanine	no activity ($<8 \times 10^{-5}$)	not measured

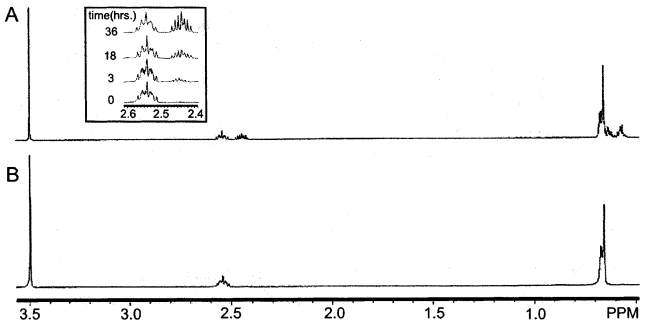

FIGURE 3: NMR analysis of the ThiO-catalyzed oxidation of *N*-cyclopropylglycine: (A) 10 mM *N*-cyclopropylglycine incubated with ThiO for 18 h and (B) 10 mM *N*-cyclopropylglycine. The inset shows the time-dependent increase in the level of cyclopropylamine with respect to *N*-cyclopropylglycine.

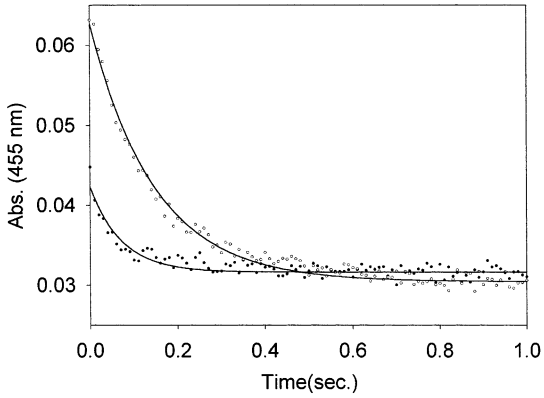

FIGURE 4: Kinetics of enzyme reduction using 200 mM glycine (●) or 200 mM deuterated glycine (○). The rates are 16.5 ± 0.5 and 6.0 ± 0.3 s^{-1}, respectively, giving an isotope effect k_H/k_D of 2.75 ± 0.5 s^{-1}.

Isotope Effect on Reduction of the Flavin. The pre-steady state deuterium isotope effect on the reduction of the flavin is 2.75 (Figure 4). Under these conditions, the reaction rate was essentially independent of glycine concentration (K_d = 31 mM).

Stereochemistry. The ThiO-catalyzed oxidation of L-alanine is at least 5000 times slower than the oxidation of D-alanine (Table 3).

Protein Architecture and Topology. ThiO is a flavoprotein consisting of two structural domains: a FAD binding domain

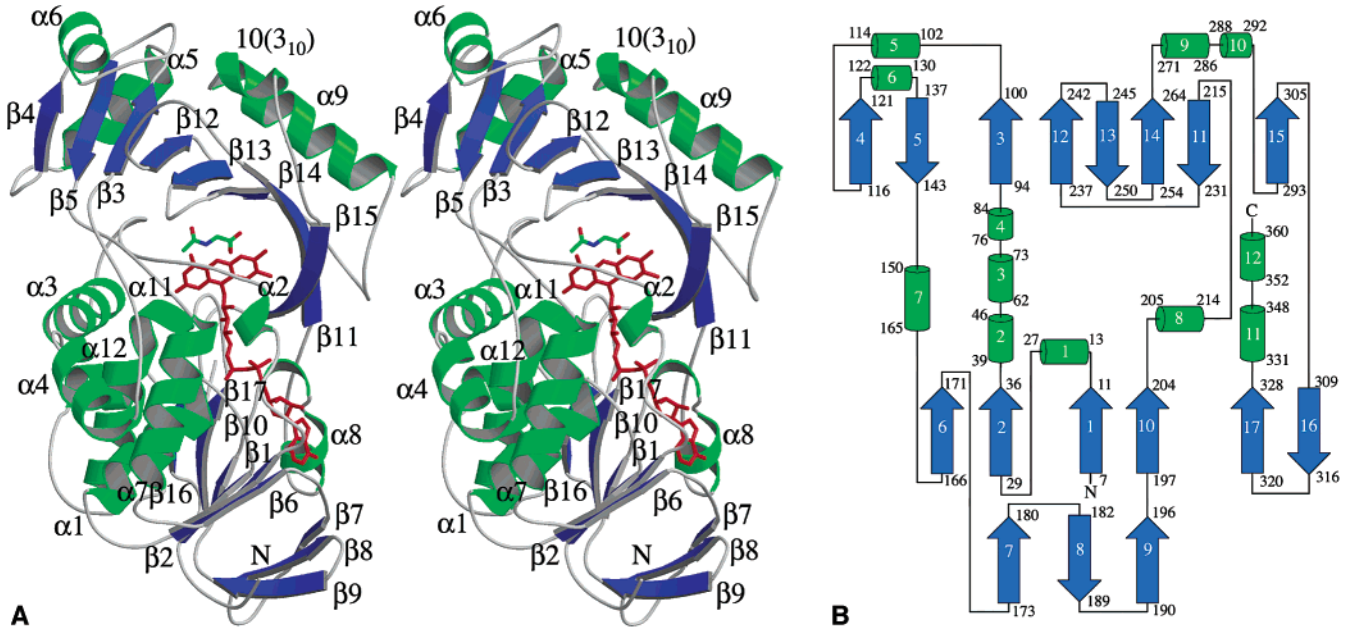

FIGURE 5: Structure of the ThiO monomer. (A) Stereoview of the ThiO monomer drawn in ribbon representation. Secondary structural elements are colored as in panel B. Ligands are shown in stick representation; FAD is colored red, and *N*-acetylglycine has carbon atoms colored green, nitrogen atoms colored blue, and oxygen atoms colored red. (B) Topology diagram of ThiO with the first and last residue number labeled for each secondary structural element. β-Strands are shown in blue, and α-helices are shown in green. Helix 10 is a 3_{10}-helix. This figure was prepared with Molscript (*33*) and Raster3D (*34*).

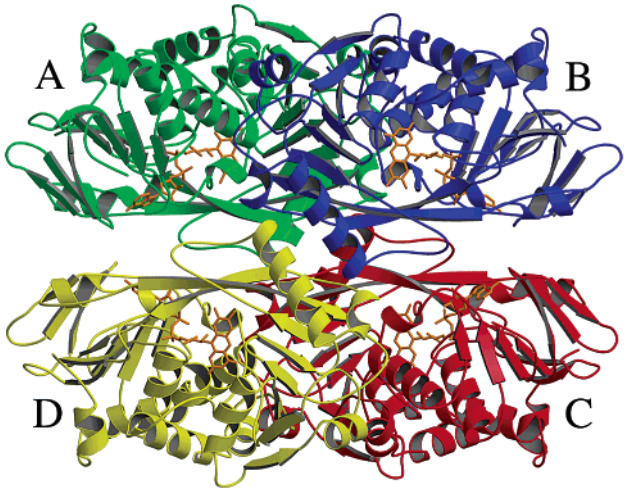

FIGURE 6: Structure of the ThiO tetramer. This view is along the crystallographic 2-fold axis with the noncrystallographic 2-fold axis vertical. Each monomer is shown in a different color. FAD is shown bound to each monomer in orange. This figure was prepared with Molscript (*33*) and Raster3D (*34*).

similar to the glutathione reductase 2 (GR_2) family (*13*) of proteins and a substrate binding domain (Figure 5). The FAD binding domain is made up of a six-stranded β-sheet with $\beta6-\beta2-\beta1-\beta10-\beta17-\beta16$ topology. The first five strands are parallel to the other five, and the edge strand ($\beta16$) is antiparallel to the other five. The sheet is flanked by a six-α-helix bundle (α1−α3−α4−α7−α11−α12) on one side and by a three-stranded β-sheet ($\beta7-\beta8-\beta9$) and α8 on the other side. The three-stranded β-sheet contains the β-meander motif characteristic of the GR_2 family FAD binding domain. Three of the helices (α1, α3, and α11) of the six-helix bundle pack against the central six-stranded β-sheet with their N-termini directed toward the FAD molecule. Helices α3 and α4 are connected by a short loop and form an outer layer of the fold. These two helices correspond to a single long helix in other family members (*7*, *8*). The substrate binding domain consists of a mixed, eight-stranded β-sheet with $\beta4-\beta5-\beta3-\beta12-\beta13-\beta14-\beta11-\beta15$ topology and flanked by helices α5, α6, and α9. Strands $\beta11$ and $\beta15$ also form part of the FAD binding site. In addition to the connections created by these two β-strands, the FAD binding domain and substrate binding domain are joined by a loop between α4 and $\beta3$ and between $\beta5$ and α7, giving a total of four crossover connections.

Quaternary Structure. ThiO is a tetramer with 222 point symmetry (Figure 6). Monomers A and C (B and D) are related by the crystallographic 2-fold axis, while the other pairs of monomers are related by noncrystallographic 2-fold axes. Each monomer of the tetramer makes contacts with the other three monomers. The main interactions between monomers A and B are hydrogen bonds that occur between helix α7 and the α3−α4 motif of one monomer and the $\beta11-\beta12$ loop and the $\beta13-\beta14$ motif of the other monomer (and the 2-fold related interactions). The A−B interface buries a total surface area of 1657 Å^2. The interface between monomers A and C involves about eight residues from α9, $\beta11$, and $\beta15$ of each monomer. This interface contains more hydrophobic interactions than the A−B interface but also contains hydrogen bonds. The A−C interface buries a total surface area of 1771 Å^2. The interface between monomers A and D utilizes residues from α8, $\beta8$, and $\beta9$. The A−D interface appears to be the weakest of the three and buries a total surface area of 809 Å^2.

The quaternary structure displays openings leading to the adenine moiety of the FAD and the glycine binding site. However, the most striking features of the quaternary structure are two buried, positively charged pockets in the interior of the protein formed by the interaction of monomers A and B and the interaction of monomers C and D (Figure 7). The pocket is lined by residues Arg89, Arg254, and

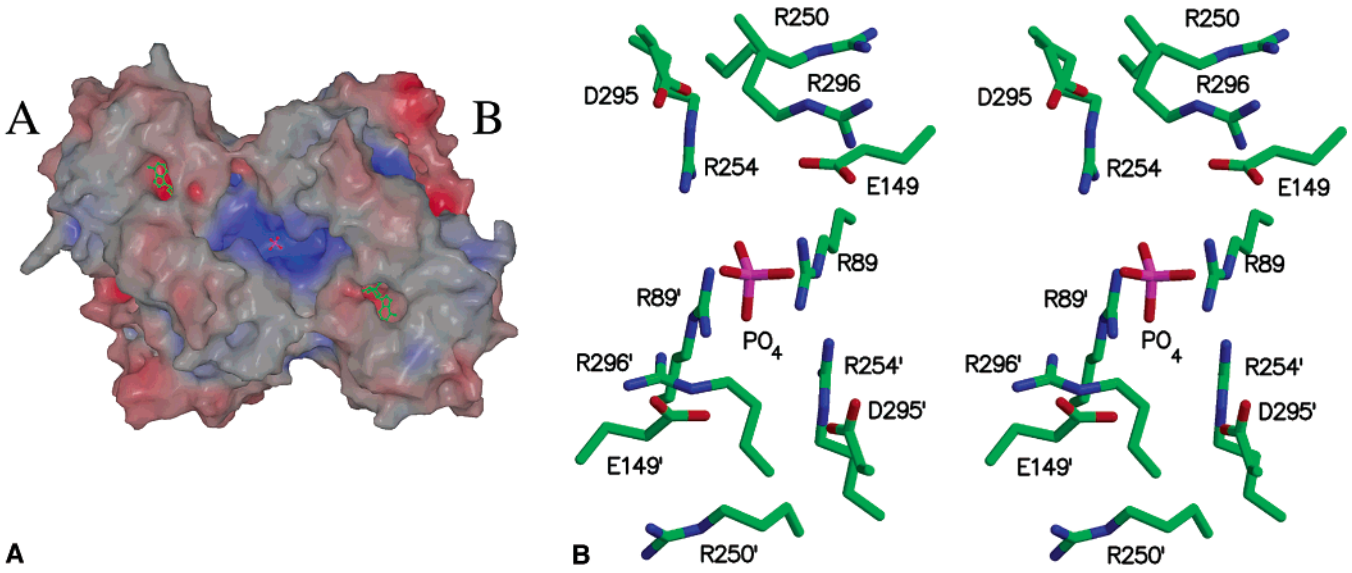

FIGURE 7: Views of the phosphate binding site. (A) Electrostatic surface representation of two monomers of ThiO viewed down the noncrystallographic 2-fold axis. Only protein atoms were considered for the surface calculation. The surface is colored blue for positively charged areas, red for negatively charged areas, and gray for neutral areas. Color saturation is proportional to the degree of electrostatic charge ranging from −25 kt to 25 kt. The phosphate (red) and FAD (green) are shown in ball-and-stick representation. (B) Stereodiagram of the charged residues in the phosphate binding region shown with the phosphate bound. Residues from both monomer A and B are shown with those from monomer B denoted with a prime after the residue number. This figure was prepared with SPOCK (*35*), Molscript (*33*), and Raster3D (*34*).

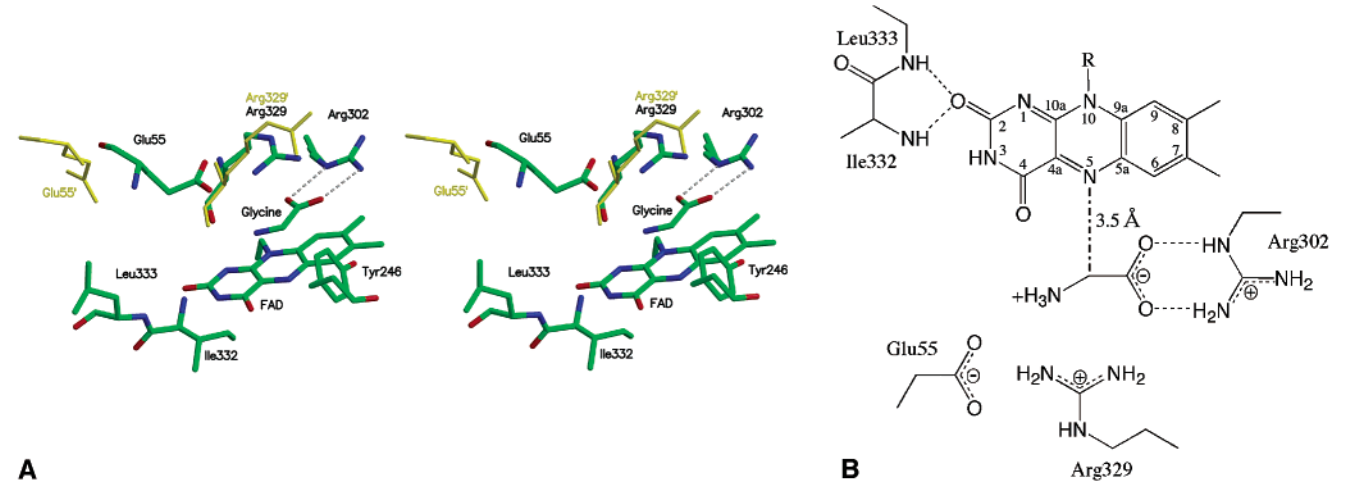

FIGURE 8: Active site of ThiO. (A) Stereoview of the active site of monomer B with glycine modeled. The active site of monomer A is superimposed on monomer B, and the only residues that show an alternate position are indicated in yellow and their numbers labeled with a prime. Only the positions of important residues are shown. For clarity, the FAD is represented by the isoalloxazine ring and the first two ribityl carbon atoms, and the only hydrogen bonds that are shown are the strongest ones to the glycine substrate. (B) Schematic diagram of the active site. The strongest hydrogen bonds (- - -) to the glycine are shown along with the potentially mechanistically important hydrogen bonds to the isoalloxazine ring of the FAD. The distance of the FAD N5 atom to the Cα atom of glycine is shown with a dashed and dotted line. This figure was prepared with Molscript (*33*) and Raster3D (*34*).

Arg296 from one monomer and the 2-fold related residues Arg89′, Arg254′, and Arg296′ from the second monomer (Figure 7A). Two negatively charged residues, Glu149 and Asp295, are located at the edge of the pocket. This pocket contained electron density on the 2-fold axis that could not be explained by the protein structure. On the basis of its size and shape, the density was modeled as a phosphate ion. The phosphate refined well and makes hydrogen bonds with Arg89 and Arg254 from each of two subunits (Figure 7B).

FAD Binding Site. FAD binds to ThiO in an extended conformation very similar to the conformation of FAD found in related FAD binding proteins (*13*). The FAD forms 17 hydrogen bonds with the protein atoms (14 main chain and three side chain) and nine additional hydrogen bonds with water molecules. The N-terminal end of the helix dipole of α11 is pointed toward the O2 position of the isoalloxazine ring, and the N-terminal end of the helix dipole of α1 is pointed toward the pyrophosphate group. These two particular dipoles are found in all of the GR_2 family members.

Substrate Binding Site. The electron density for crystals treated with *N*-acetylglycine showed one *N*-acetylglycine molecule per subunit (Figure 8A). The Cα atom, amino group, and carboxylate group are well-ordered, but the acetyl group is less clear in the electron density. The *N*-acetylglycine is bound on the *re* side of the isoalloxazine ring. One carboxylate oxygen atom forms a hydrogen bond to the NE atom of Arg302, while the other forms a hydrogen bond with NH2 of Arg302. The acetyl group is near the guanidinium

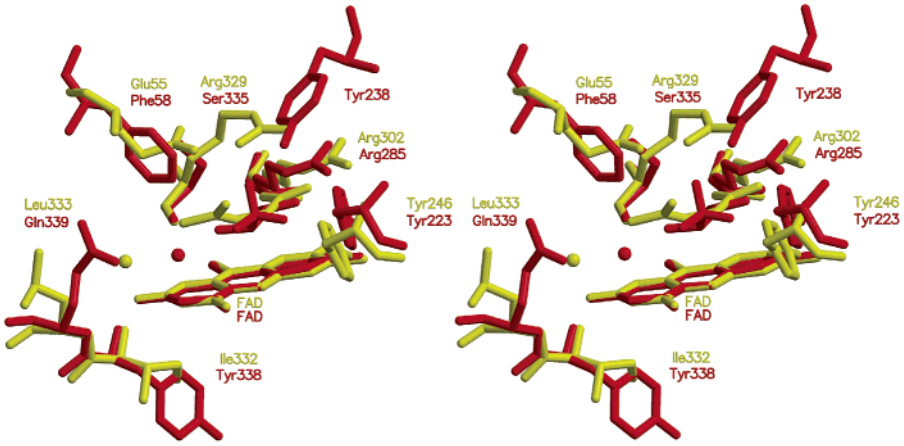

FIGURE 9: Superposition of the active site of ThiO and rgDAAOX. Residues found in structurally similar locations in the *N*-acetylglycine-bound structure of ThiO and the trifluoroalanine-bound structure of rgDAAOX (1COL) are shown with their respective ligands. ThiO is shown in yellow, and rgDAAOX is shown in red. Each has a water bound near the active site which is shown as a sphere. Only the isoalloxazine ring and a ribitoyl carbon atom of the FAD are shown for clarity. This figure was prepared with Molscript (*33*) and Raster3D (*34*).

group of Arg329. The positioning of the glycine places the Cα atom ~3.5 Å from the N(5) atom of the isoalloxazine ring (Figure 8B). In one monomer, Glu55 is located near the active site and forms a bifurcated hydrogen bond with the NH1 atom of Arg329, while in the other monomer, Glu55 is pointed away from the active site and Arg329 is slightly rotated away from the active site (Figure 8A).

DISCUSSION

Comparison of ThiO to Related Enzymes. A search of the DALI structural database (*25*) showed that ThiO is most similar in overall structure to sarcosine oxidase (SOX) (*7*) followed by D-amino acid oxidase (DAAOX) (*8*). SOX showed an rms difference of 2.3 Å for 350 of 385 amino acids with 20% identity, while DAAOX showed an rms difference of 2.5 Å for 298 of 340 amino acids with 17% identity. Other FAD-dependent amine oxidases (e.g., aspartate oxidase, L-amino acid oxidase, and polyamine oxidase) show less structural similarity. These and other FAD-dependent enzymes showed fewer amino acid matches or higher rms deviations. Searching the DALI database with only the FAD binding domain or with only the substrate binding domain showed similar trends; however, the substrate binding domain of ThiO is more similar to DAAOX, while the FAD binding domain of ThiO is more similar to SOX.

The GR family of FAD binding proteins is characterized by a five-stranded parallel β-sheet flanked by two α-helices. These two helices and the first three strands form a Rossmann fold. A second three-stranded antiparallel β-sheet forms a crossover between the Rossmann fold and the remaining two strands, creating a $\beta\beta\alpha$ sandwich (*13*). The GR family can be divided into two subfamilies, GR_1 and GR_2. The FAD binding domain of ThiO belongs to the GR_2 family. The FAD binding residues in the GR_2 family show little sequence identity. The signature sequence $GxGxxG(x)_{17}E$ is found for ThiO beginning at Gly11 and ending at Glu34. Glu34 provides hydrogen bond acceptors for the 2′-hydroxyl group of the adenosyl moiety of the cofactor. Because most of the interactions with FAD occur between main chain atoms or water molecules, sequence identity is not necessarily a good indicator of structural similarity. Overall, the FAD binding domain of ThiO has interactions with residues that are more similar to those of DAAOX than those of SOX.

The substrate binding domain of ThiO is most similar to that of DAAOX (Figure 9). The main substrate binding interaction occurs between Arg302 and the carboxylate group of *N*-acetylglycine via a pair of hydrogen bonds. Corresponding arginine residues are found in pig kidney DAAOX (pkDAAOX) (Arg283) (*8*) and in *Rhodotorula gracilis* DAAOX (rgDAAOX) (Arg285) (*9*), and this arginine is conserved among the known ThiO sequences. Both ThiO and DAAOX contain a tyrosine residue near the carboxylate group of the substrate. The structurally similar residue in ThiO, Tyr246, does not appear to form a hydrogen bond with *N*-acetylglycine but could do so with the substrate glycine by a repositioning of its side chain. Tyr246 is also conserved in all of the known ThiO sequences.

Three additional residues, Arg329, Met261, and Glu55, are located near the active site and show conformational differences between the ThiO and the ThiO−*N*-acetylglycine structures. All three residues are completely conserved in the known ThiO sequences. The position of Arg329 is usually occupied by a small residue such as Gly313 (pkDAAO) (*8*) or Ser335 (rgDAAOX) (*9*), or a residue that is offset from the active site, such as His345 (SOX) (*7*) in other amine oxidases. Met261 is near Arg302, and its conformation appears to be linked to that of Arg329. Glu55 is part of a flexible loop from residue 54 to 60. In the unliganded ThiO, Glu55 is pointed away from the active site. After the inhibitor has bound, the loop is more ordered but shows a difference between monomers A and B. In monomer B, Glu55 forms a strong hydrogen bond with Arg329, resulting in a lid that covers the substrate binding site. In monomer A, Glu55 is oriented toward the active site but does not form a hydrogen bond with Arg329. It is possible that the structural differences beween monomers A and B are the result of crystal contacts that involve the loop of monomer A. The lid formed by Glu55 and Arg329 might serve to protect the imine product from hydrolysis before it is released for the next step of thiazole biosynthesis.

Despite the high degree of structural similarity of ThiO and SOX and the similarity of the substrates glycine and

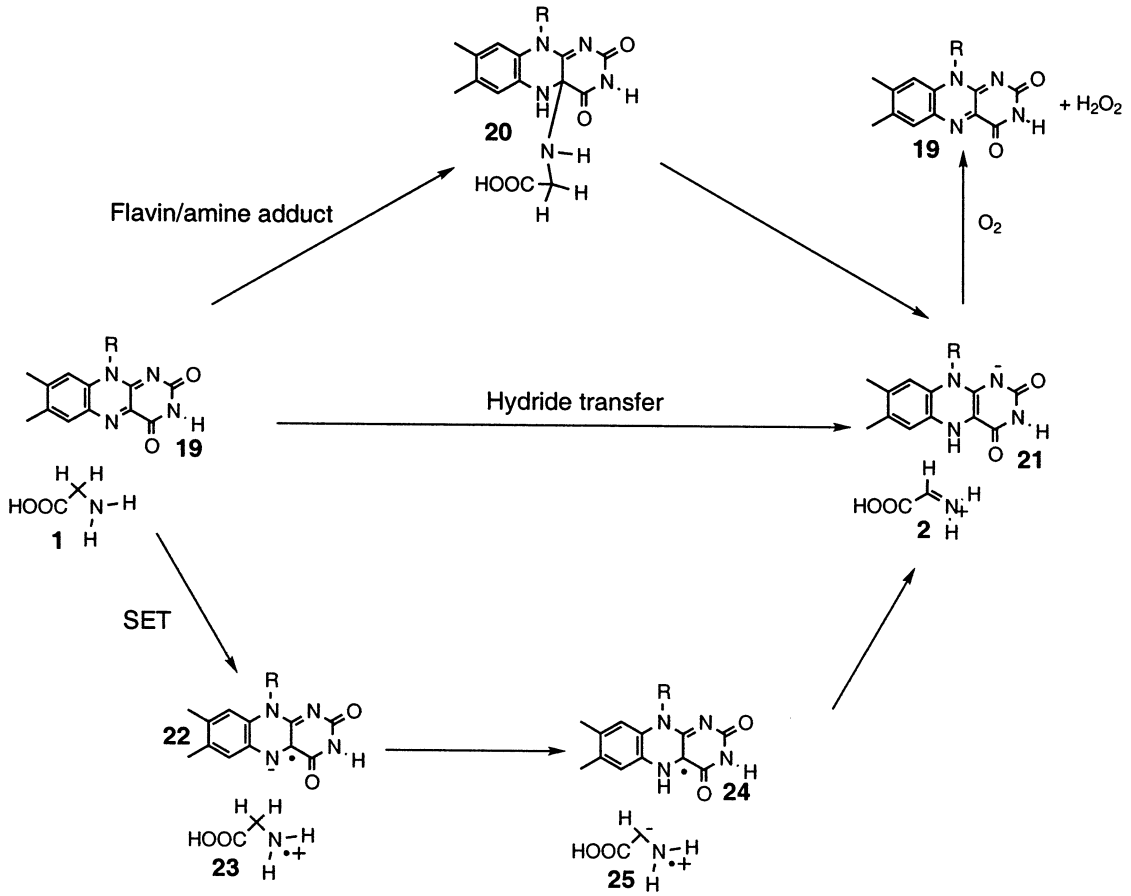

FIGURE 10: Mechanistic proposals for the flavin-catalyzed oxidation of amines.

sarcosine, the substrate binding geometry in ThiO is reversed compared to that reported for SOX. In both geometries, the carboxylate group hydrogen bonds to an arginine side chain; however, it is positioned above C2 of the isoalloxazine ring in SOX, and above C8 in ThiO. Thus, while the structure of ThiO is more closely related to the structure of SOX, substrate binding to ThiO is more similar to substrate binding to DAAOX.

Thus far, the reported quaternary structures of the GR_2 family proteins are either monomers or dimers. The biologically active form of DAAOX (*8*, *9*), phenol hydroxylase (*26*), and monoamine oxidase (*27*) are all dimers, while SOX (*7*) and polyamine oxidase (*11*) are monomers. In general, the subunit−subunit interactions for the dimeric proteins tend to involve the substrate binding domains rather than the FAD binding domains; however, none of the dimer contacts are similar. ThiO is the first example of a tetrameric GR_2 family member. Although most of the tetrameric contacts involve the substrate binding domain, there is some participation of the FAD binding domains. When the domains are dissected into three possible dimers (A−B, A−C, or A−D), no similarity is detected between dimeric contacts in ThiO with the other GR_2 dimers. For ThiO, formation of the tetramer results in a buried, electropositive cavity. The role of this cavity is not known, and no similar cavities are found in the GR_2 dimers. Furthermore, the arginine residues that line this cavity are not conserved.

Role of ThiO in Thiamin Biosynthesis. ThiO from *B. subtilis* is an essential enzyme in the biosynthesis of the thiazole moiety of thiamin because a *thiO*$^-$ mutant has an absolute requirement for the thiazole alcohol (dephospho **12** in Figure 1). In addition, we have demonstrated that ThiO is essential for the cell free reconstitution of the thiazole biosynthesis (unpublished). These experimental observations confirm the prediction, based on the clustering of *thiO* with *thiS*, *thiG*, and *thiF*, that this protein is involved in some aspect of thiamin biosynthesis.

Mechanistic Proposal for Glycine Oxidase. A schematic representation of the active site of glycine oxidase, showing bound glycine and the residues that appear from the structure to play a key role in catalysis, is shown in Figure 8. The glycine is located on the *re* face of the flavin with the pro-*S* hydrogen of the substrate suitably positioned for transfer to the flavin. This is in agreement with the stereochemical experiment in which replacement of the pro-*S* hydrogen of glycine with a methyl group in L-Ala prevents the oxidation, while a similar replacement of the pro-*R* hydrogen does not. There is no protein base close to the Cα atom of the substrate, and the reduced flavin ($FADH^-$) is stabilized by hydrogen bonding of O2 to the amide protons of Ile332 and Leu333.

Flavin-mediated oxidation of amines has been extensively studied, and the three different mechanisms currently described in the literature (*28*−*30*) are summarized in Figure 10.

In the hydride transfer mechanism, the nitrogen lone pair facilitates the transfer of a hydride to N5 of the flavin. This mechanism is consistent with all the available data on glycine oxidase. The pro-*S* hydrogen of *N*-acetylglycine is positioned almost directly above N5 of the flavin with a Cα−N5 distance of 3.5 Å. This appears to be the stereoelectronically

favored position for hydride transfer because the same orientation between N5 and the transferred hydrogen is found in pyridoxine 5′-phosphate oxidase (*31*) and dihydroorotate dehydrogenase (*32*), two other enzymes that are likely to proceed by hydride transfer mechanisms. Further support for the hydride transfer mechanism comes from the observation that cyclopropylglycine is a good substrate for the enzyme and not a suicide substrate as would be expected for a single-electron transfer (SET) mechanism (see below). In addition, the large pre-steady state deuterium isotope effect of 2.75 on the flavin reduction is consistent with this proposal.

The second mechanistic hypothesis involves addition of the amine to the C4a atom of the flavin followed by an elimination reaction. While the amide nitrogen atom of *N*-acetylglycine is suitably positioned for this addition, the E2 elimination to form the imine requires a base positioned close to the Cα atom of glycine and *trans* periplanar to the N5−C4a bond. The absence of such a base in glycine oxidase makes this mechanism unlikely.

The SET mechanism involves an initial electron transfer from the amine to the flavin to give the amine radical cation **23** and the flavin semiquinone **22**. Deprotonation of the amine radical cation, protonation of the flavin semiquinone, and a final electron transfer to the protonated flavin semiquinone **24** would complete the reaction. If it is assumed that N5 of the flavin semiquinone **22** can function as the base to deprotonate the glycine radical cation **23**, the glycine oxidase structure is consistent with the SET mechanism. However, the observation that cyclopropylglycine is oxidized without enzyme inactivation or ring opening (Figure 3) does not support this mechanism.

Proposed Role for Glycine Oxidase in Thiazole Biosynthesis. A mechanistic proposal for the role of ThiO in the formation of the thiazole moiety of thiamin is outlined in Figure 1. In this proposal, ThiO-catalyzed oxidation of glycine would give imine **2**. Trapping of this imine with ThiS thiocarboxylate, a previously characterized intermediate (*5*), would give **4**. This nucleophilic addition might occur at the active site of ThiO to avoid the nonproductive hydrolysis of **2** that would occur if it were released from the enzyme. Addition of the amino group of **4** to the carbonyl group of DXP (**5**) would yield imine **6**, which could then tautomerize by a protonation−deprotonation sequence to give **7**. Hydrolysis of the thioester of **7** would activate the thiol group, which could then undergo an intramolecular addition to the carbonyl group of **8** to form **9**. Two dehydrations, the first to form **10** and the second to form **11** followed by a decarboxylation, would complete the biosynthesis of the thiazole phosphate **12**.

An alternative mechanism in which glycine first forms an imine with DXP (**5**) is unlikely because the active site is not sufficiently large to accommodate the DXP−glycine adduct **14**.

Conclusions. The *thiO* gene of *B. subtilis* encodes an FAD-dependent glycine oxidase. This enzyme is essential for the biosynthesis of the thiazole moiety of thiamin pyrophosphate. Here we describe the structure of ThiO with *N*-acetylglycine bound at the active site. The closest structural relatives are sarcosine oxidase and D-amino acid oxidase. This structure and additional mechanistic studies are consistent with a hydride transfer mechanism for glycine oxidation. The deuterium isotope effect on flavoenzyme reduction is 2.75, and the pro-*S* glycine hydrogen is suitably positioned for transfer to N5 on the *re* face of the flavin. In addition, ThiO catalyzed the oxidation of *N*-cyclopropylglycine without ring opening or inactivation, suggesting that the oxidation is not proceeding via radical intermediates. ThiO does not catalyze the oxidation of glycine analogues designed to mimic a DXP−glycine adduct. This limits the mechanistic possibilities for the role of ThiO in thiazole biosynthesis.

REFERENCES

1. Begley, T. P., Downs, D. M., Ealick, S. E., McLafferty, F. W., Van Loon, A. P., Taylor, S., Campobasso, N., Chiu, H. J., Kinsland, C., Reddick, J. J., and Xi, J. (1999) *Arch. Microbiol. 171*, 293−300.
2. Lauhon, C. T., and Kambampati, R. (2000) *J. Biol. Chem. 275*, 20096−20103.
3. Miranda-Rios, J., Morera, C., Taboada, H., Davalos, A., Encarnacion, S., Mora, J., and Soberon, M. (1997) *J. Bacteriol. 179*, 6887−6893.
4. Xi, J., Ge, Y., Kinsland, C., McLafferty, F. W., and Begley, T. P. (2001) *Proc. Natl. Acad. Sci. U.S.A. 98*, 8513−8518.
5. Taylor, S. V., Kelleher, N. L., Kinsland, C., Chiu, H. J., Costello, C. A., Backstrom, A. D., McLafferty, F. W., and Begley, T. P. (1998) *J. Biol. Chem. 273*, 16555−16560.
6. Nishiya, Y., and Imanaka, T. (1998) *FEBS Lett. 438*, 263−266.
7. Trickey, P., Wagner, M. A., Jorns, M. S., and Mathews, F. S. (1999) *Structure 7*, 331−345.
8. Mattevi, A., Vanoni, M. A., Todone, F., Rizzi, M., Teplyakov, A., Coda, A., Bolognesi, M., and Curti, B. (1996) *Proc. Natl. Acad. Sci. U.S.A. 93*, 7496−7501.
9. Umhau, S., Pollegioni, L., Molla, G., Diederichs, K., Welte, W., Pilone, M. S., and Ghisla, S. (2000) *Proc. Natl. Acad. Sci. U.S.A. 97*, 12463−12468.
10. Mattevi, A., Tedeschi, G., Bacchella, L., Coda, A., Negri, A., and Ronchi, S. (1999) *Structure Folding Des. 7*, 745−756.
11. Binda, C., Coda, A., Angelini, R., Federico, R., Ascenzi, P., and Mattevi, A. (1999) *Structure 7*, 265−276.
12. Job, V., Molla, G., Pilone, M. S., and Pollegioni, L. (2002) *Eur. J. Biochem. 269*, 1456−1463.
13. Dym, O., and Eisenberg, D. (2001) *Protein Sci. 10*, 1712−1728.
14. Errington, J. (2002) http://locus.jouy.inra.fr/cgi-bin/genmic/madbase/progs/ACCUEIL-MUTANT.pl.
15. Bradford, M. M. (1976) *Anal. Biochem. 72*, 248−254.
16. Otwinowski, Z., and Minor, W. (1997) *Methods Enzymol. 276*, 307−326.
17. *MOSFLM*, version 5.40 (1997) MRC Laboratory of Molecular Biology, Cambridge, U.K.
18. *SCALA*, version 3.3 (1993) MRC Laboratory of Molecular Biology, Cambridge, U.K.
19. Miller, R., DeTitta, G. T., Jones, R., Langs, D. A., Weeks, C. M., and Hauptman, H. A. (1993) *Science 259*, 1430−1433.
20. Miller, R., Gallo, S. M., Khalak, H. G., and Weeks, C. M. (1994) *J. Appl. Crystallogr. 27*, 613−621.
21. Smith, G. D., Nagar, B., Rini, J. M., Hauptman, H. A., and Blessing, R. H. (1998) *Acta Crystallogr. D54*, 799−804.
22. Brünger, A. T., Adams, P. D., Clore, G. M., DeLano, W. L., Gros, P., Grosse-Kunstleve, R. W., Jiang, J. S., Kuszewski, J., Nilges, M., Pannu, N. S., Read, R. J., Rice, L. M., Simonson, T., and Warren, G. L. (1998) *Acta Crystallogr. D54*, 905−921.
23. Jones, T. A., Zou, J.-Y., Cowan, S. W., and Kjeldgaard, M. (1991) *Acta Crystallogr. A47*, 110−119.
24. Kleygert, G. J., and Jones, T. A. (1996) *Acta Crystallogr. D52*, 826−828.
25. Holm, L., and Sander, C. (1993) *J. Mol. Biol. 233*, 123−138.
26. Enroth, C., Neujahr, H., Schneider, G., and Lindqvist, Y. (1998) *Structure 6*, 605−617.
27. Binda, C., Newton-Vinson, P., Hubalek, F., Edmondson, D. E., and Mattevi, A. (2001) *Nat. Struct. Biol. 26*, 26.
28. Miller, J. R., and Edmondson, D. E. (1999) *Biochemistry 38*, 13670−13683.
29. Silverman, R. B. (1995) *Acc. Chem. Res. 28*, 335−342.
30. Zhao, G., Qu, J., Davis, F. A., and Jorns, M. S. (2000) *Biochemistry 39*, 14341−14347.
31. Safo, M. K., Musayev, F. N., di Salvo, M. L., and Schirch, V. (2001) *J. Mol. Biol. 310*, 817−826.

32. Rowland, P., Bjornberg, O., Nielsen, F. S., Jensen, K. F., and Larsen, S. (1998) *Protein Sci. 7*, 1269−1279.
33. Kraulis, P. J. (1991) *J. Appl. Crystallogr. 24*, 946−950.
34. Merritt, E. A., and Bacon, D. J. (1997) *Methods Enzymol. 277*, 505−524.
35. Christopher, J. A. (1998) *SPOCK*, Texas A&M University, College Station, TX.

BI026916V